Experimental Investigation of Propeller Aerodynamic Derivatives

Jiří Čečrdle*†

* VZLU AEROSPACE, a.s.

Beranových 130, Prague, 19900, Czechia
cecrdle@vzlu.cz

† Corresponding Author

Abstract

Submitted paper is focused on the experimental determination of the propeller aerodynamic derivatives that are used for the analysis of whirl flutter. Whirl flutter is a specific type of flutter instability that is driven by motion-induced unsteady aerodynamic propeller forces and moments acting in the propeller plane. To determine the forces and moments acting at the propeller disc, propeller aerodynamic derivatives are used. The analytical solution of derivatives is unreliable, and therefore, experimental validation of the selected derivatives is required. Paper describes the mechanical concept of the used demonstrator that represents a sting-mounted nacelle with a motor and propeller with two degrees-of-freedom (engine pitch and yaw). The main focus is paid on the test including the list of the tested variants, methodology of testing and the data assessment. Finally, the examples of the results are provided.

1. Introduction

Whirl flutter is a specific type of aeroelastic flutter instability, which may appear on turboprop aircraft due to the effect of rotating parts, such as a propeller or a gas turbine engine rotor. Rotating mass generates additional forces and moments and increases the number of degrees-of-freedom. Rotating propellers also cause an aerodynamic interference effect between a nacelle and a wing. Whirl flutter instability is driven by motion-induced unsteady aerodynamic propeller forces and moments acting at the propeller plane. It may cause unstable vibration, which can lead to failure of an engine installation or an entire wing.

The propeller whirl flutter phenomenon was analytically discovered by Taylor and Browne in 1938 [1]. The next pioneering work was performed by Ribner, who set the basic formulae for the aerodynamic derivatives of propeller forces and moments due to the motion and velocities in pitch and yaw in 1945 [2, 3]. After the accidents of two Lockheed L-188 C Electra II airliners in 1959 and 1960 [4], the importance of the whirl flutter phenomenon on practical applications was recognized.

The complicated physical principle of whirl flutter requires experimental validation of the analytical results, especially due to the unreliable analytical solution of the propeller aerodynamic forces. Further, structural damping is a key parameter, to which whirl flutter is extremely sensitive and which needs to be validated. Therefore, aeroelastic models are used. The important experiments were carried out in NASA Langley by Reed, Bennett, Kvaternik and many others [5 - 10]. Experimental research into whirl flutter is also reported in [11]. A comprehensive description of whirl flutter experimental research is provided in [12].

The aeroelastic demonstrator for the experimental research into the whirl flutter phenomenon (W-WING), developed at the VZLU represents the half-wing and engine of a typical commuter turboprop aircraft structure. The model includes a nacelle with a powered propeller [13]. This demonstrator has been used for the measurements of the whirl flutter stability in the frame of past projects [14, 15]. Further measurements are planned within the subjected OFELIA project.

For the investigation of aerodynamic derivatives, the new option of the demonstrator representing a sting-mounted nacelle with a motor and a powered propeller (W-STING) has been developed.

2. Theoretical Background

The principle of the whirl flutter phenomenon is outlined on a simple mechanical system with two degrees-of-freedom [12]. The propeller and hub are considered to be rigid. A flexible engine mounting is substituted as a system of two rotational springs (stiffness K_{Ψ} , K_{Θ}), as illustrated in figure 1.

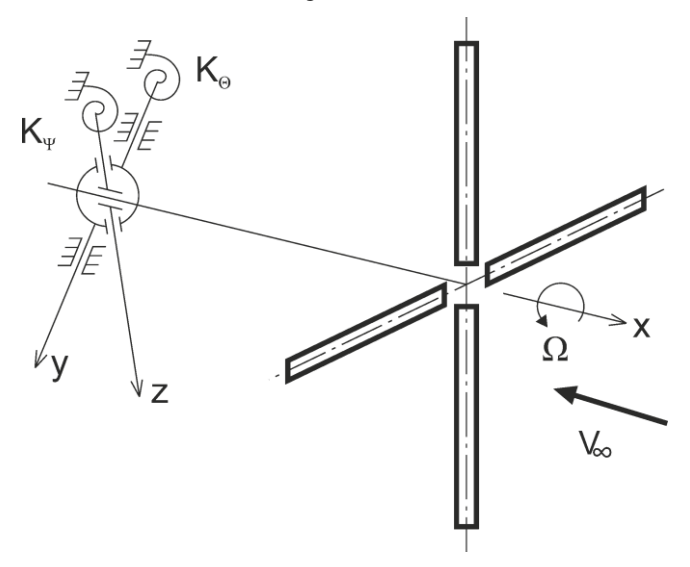


Figure 1: Gyroscopic system with a propeller.

Such a system has two independent mode shapes of yaw and pitch, with respective angular frequencies of ω_{Ψ} and ω_{Θ} . Considering the propeller rotation with angular velocity Ω , the primary system motion changes to the characteristic gyroscopic motion. The gyroscopic effect causes two independent mode shapes to merge into whirl motion. The propeller axis develops an elliptical movement. The trajectory of this elliptical movement depends on both angular frequencies ω_{Ψ} and ω_{Θ} . The orientation of the propeller axis movement is backward relative to the propeller rotation for the lower-frequency mode (backward whirl mode) and is forward relative to the propeller rotation for the higher-frequency mode (forward whirl mode). Because the yaw and pitch motions have a 90° phase shift, the mode shapes in the presence of gyroscopic effects are complex.

The described gyroscopic motion causes the angles of attack of the propeller blades to change, which consequently leads to unsteady aerodynamic forces. These forces may, under specific conditions, induce whirl flutter instability. The flutter state is defined as neutral stability with no damping of the system, and the corresponding airflow ($V = V_{FL}$) is called the critical flutter speed. The possible states of the gyroscopic system from a flutter point of view for the backward mode are explained in figure 2. Provided that the air velocity is lower than a critical value ($V < V_{FL}$), the system is stable, and the gyroscopic motion is damped. If the airspeed exceeds the critical value ($V > V_{FL}$), then the system becomes unstable and gyroscopic motion is divergent.

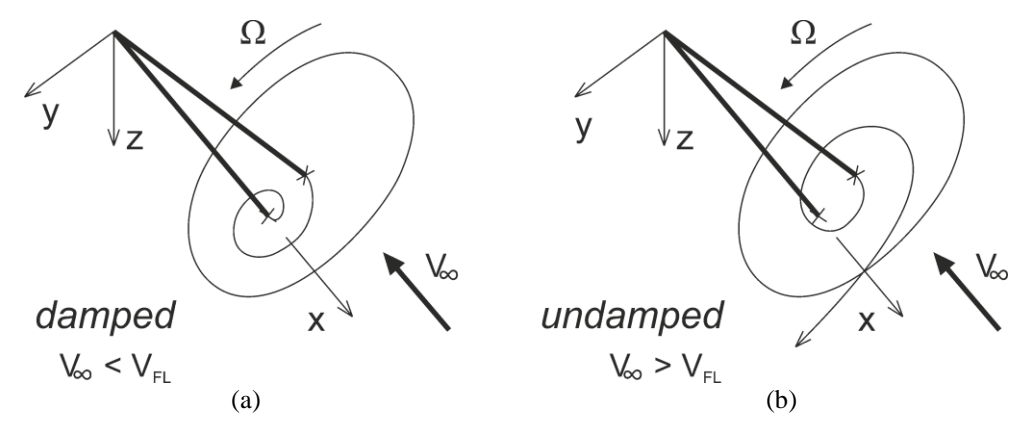


Figure 2: Stable (a) and unstable (b) state of gyroscopic vibrations for the backward flutter mode.

The analytical solution is intended to determine the aerodynamic force caused by the gyroscopic motion on each of the

propeller blades. The presented equations of motion were derived for the system shown in figure 1 using Lagrange's approach. The kinematical scheme including gyroscopic effects is shown in figure 3. We select three angles (ϕ, Θ, Ψ) as the independent generalized coordinates. The propeller angular velocity is considered to be constant $(\phi = \Omega t)$. The rotating component is assumed to be cyclically symmetric with respect to both mass and aerodynamics (i.e., a propeller with a minimum of three blades). Non-uniform mass moments of inertia of the engine with respect to pitch and yaw axes $(J_Z \neq J_Y)$ are also considered.

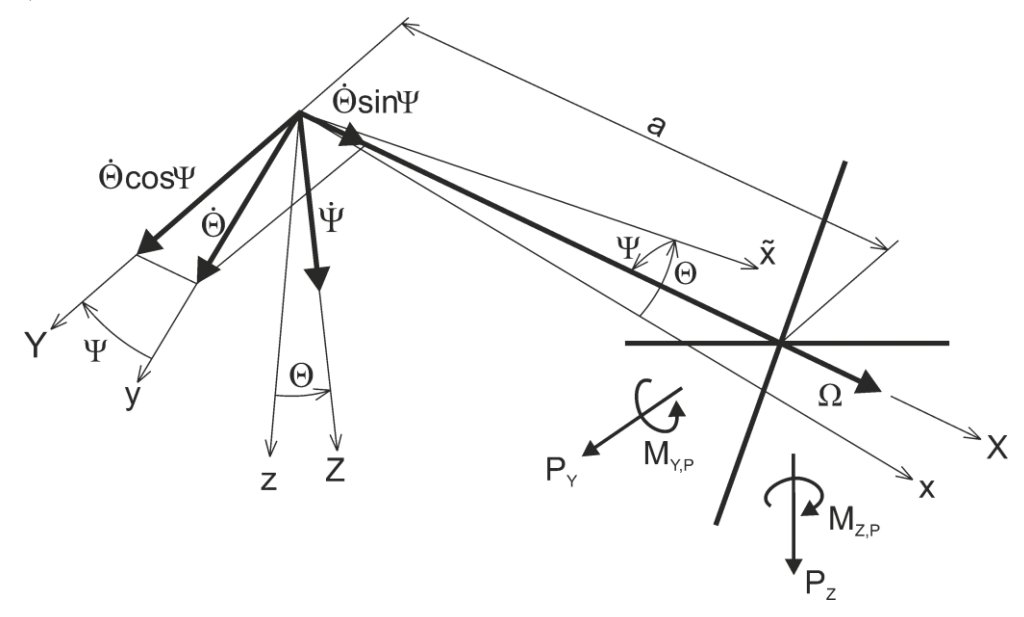


Figure 3: Kinematical scheme of the gyroscopic system

Considering small angles, the equations of motion become:

$$J_{Y}\ddot{\Theta} + (K_{\Theta}\gamma_{\Theta}/\omega)\dot{\Theta} + J_{X}\Omega\dot{\Psi} + K_{\Theta}\Theta = M_{YP} - aP_{Z}$$

$$J_{Z}\ddot{\Psi} + (K_{\Psi}\gamma_{\Psi}/\omega)\dot{\Psi} + J_{X}\Omega\dot{\Theta} + K_{\Psi}\Psi = M_{ZP} + aP_{Y}$$
(1)

Propeller aerodynamic forces (right-hand side of eqn. 1, see also figure 3) are determined using aerodynamic derivatives [3, 16]. Neglecting the aerodynamic inertia terms, the equations for the propeller's dimensionless forces and moments may be expressed as follows:

$$P_{Y} = qS\left(c_{y\Psi}\Psi^{*} + c_{y\Theta}\Theta^{*} + c_{yq}(\dot{\Theta}^{*}D/2V)\right) \qquad P_{Z} = qS\left(c_{z\Psi}\Psi^{*} + c_{z\Theta}\Theta^{*} + c_{zr}(\dot{\Psi}^{*}D/2V)\right)$$

$$M_{YP} = qSD\left(c_{m\Psi}\Psi^{*} + c_{mq}(\dot{\Theta}^{*}D/2V)\right) \qquad M_{ZP} = qSD\left(c_{n\Theta}\Theta^{*} + c_{nr}(\Psi^{*}D/2V)\right)$$
(2)

Where \mathbf{q} is a dynamic pressure, \mathbf{S} is a propeller disc area, \mathbf{D} is a propeller diameter and \mathbf{V} is an airflow velocity. The aerodynamic derivatives (c-terms) are defined as follows:

$$c_{y\Theta} = \partial c_{y}/\partial \Theta^{*} \quad c_{y\Psi} = \partial c_{y}/\partial \Psi^{*} \quad c_{yq} = \partial c_{y}/\partial (\dot{\Theta}D/2V) \quad c_{yr} = \partial c_{y}/\partial (\dot{\Psi}D/2V)$$

$$c_{z\Theta} = \partial c_{z}/\partial \Theta^{*} \quad c_{z\Psi} = \partial c_{z}/\partial \Psi^{*} \quad c_{zq} = \partial c_{z}/\partial (\dot{\Theta}D/2V) \quad c_{zr} = \partial c_{z}/\partial (\dot{\Psi}D/2V)$$

$$c_{m\Theta} = \partial c_{m}/\partial \Theta^{*} \quad c_{m\Psi} = \partial c_{m}/\partial \Psi^{*} \quad c_{mq} = \partial c_{m}/\partial (\dot{\Theta}D/2V) \quad c_{mr} = \partial c_{m}/\partial (\dot{\Psi}D/2V)$$

$$c_{n\Theta} = \partial c_{n}/\partial \Theta^{*} \quad c_{n\Psi} = \partial c_{n}/\partial \Psi^{*} \quad c_{nq} = \partial c_{n}/\partial (\dot{\Theta}D/2V) \quad c_{nr} = \partial c_{n}/\partial (\dot{\Psi}D/2V)$$
(3)

Considering the symmetry (or antisymmetry), we can reduce the number of derivatives as follows:

$$c_{z\Psi} = c_{y\Theta}; c_{m\Psi} = -c_{n\Theta}; c_{mq} = c_{nr}; c_{zr} = c_{yq}; c_{z\Theta} = -c_{y\Psi}; c_{n\Psi} = c_{m\Theta}; c_{mr} = -c_{nq}; c_{yr} = -c_{zq}$$
(4)

In addition, we can neglect the negligible derivatives: $\mathbf{c}_{mr} = -\mathbf{c}_{nq} = \mathbf{0}$ and $\mathbf{c}_{yr} = -\mathbf{c}_{zq} = \mathbf{0}$. Finally, we obtained six

independent derivatives: $\mathbf{c}_{Z\Theta}$, $\mathbf{c}_{m\Theta}$, $\mathbf{c}_{Z\Psi}$, $\mathbf{c}_{m\Psi}$, \mathbf{c}_{mq} and \mathbf{c}_{zr} . The first four ones may be investigated experimentally. Final solving for the critical (flutter) state assuming harmonic motion has the character of an eigenvalue problem. The final whirl flutter matrix equation can be expressed as:

$$\left(-\omega^2[M] + j\omega\left([D] + [G] + qS\frac{D}{V}[D^A]\right) + ([K] + qSD[K^A])\right)\left[\frac{\overline{\Theta}}{\overline{\Psi}}\right] = \{0\}$$
 (5)

Where [M], [D] and [K] are structural mass, damping and stiffness matrix, respectively while [D^A] and [K^A] are aerodynamic damping and stiffness matrix, respectively. Finally, [G] is gyroscopic matrix and $\overline{\theta}$, $\overline{\Psi}$ are generalized pitch and yaw angles, respectively. The critical state emerges when the angular velocity ω is real. The critical state can be reached by increasing either V or Ω . Increasing the propeller advance ratio $(V/(\Omega R))$ has a destabilizing effect. Another important parameter is the distance between the propeller and the node points of the engine vibration modes. Structural damping is a significant stabilization factor, while in contrast, the influence of the propeller thrust is negligible. The small influence of the propeller thrust derives from the fact that the variance of the aerodynamic derivatives of the thrusted propeller and windmilling propeller can be high in the low-speed region, but at high velocities (where whirl flutter is expected), the variance is less than 5% [6]. The most critical state is $\omega_{\theta} = \omega_{\Psi}$, when the interaction of both independent motions is maximal, and the trajectory of the gyroscopic motion is circular. Considering rigid propeller blades, the whirl flutter inherently appears in the backward gyroscopic mode. A special case of eqn. 5 for $\omega = 0$ is gyroscopic static divergence, which is characterized by uni-directional divergent motion. The described mathematical model that considers a rigid propeller is obviously applicable to conventional propellers, for which the propeller blade frequencies are much higher compared to the nacelle pitch and yaw frequencies.

3. W-STING Demonstrator

Aeroelastic demonstrator for investigation of a propeller aerodynamic derivatives (W-STING) represents a sting-mounted nacelle with a motor and propeller. The demonstrator includes two degrees-of-freedom (engine pitch and yaw). For the measurement, just a single degree-of-freedom is used, and the other one is mechanically blocked. The stiffness parameters in both pitch and yaw are modelled by means of cross spring pivots with changeable spring leaves. Stiffness constants are independently adjustable by replacing these spring leaves. The leaf spring thickness ranges from 2.0 to 3.5 mm. The corresponding effective stiffness of the pitch hinge ranges from 246.4 to 1320.5 Nm.rad⁻¹ and the engine pitch frequency ranges from 1.96 to 4.54 Hz. Both pivots can be independently moved in the direction of the propeller axis within the range of 0.15 m to adjust the pivot points of both vibration modes. The inertia of the engine is modeled by the movable (sliding) weight. The range of balance weight stations is 0.208 m. The plastic nacelle cowling is manufactured using 3D print technology.

The gyroscopic effect of the rotating mass is simulated by the mass of the propeller blades. Two sets of blades made of duralumin and steel are available. The polar moment of inertia of propeller with duralumin and steel blades is 0.0266 kg.m^2 and 0.0659 kg.m^2 , respectively. The propeller with $\mathbf{D} = 0.7$ m represents a scaled-down real Avia V-518 5-blade propeller. The propeller blades' angle of attack is adjustable at the standstill by means of the special tool. The propeller is powered by an electric motor with a nominal power of 15 kW. The power is sufficient to provide the measurement with the propeller in thrust mode. The demonstrator sensor instrumentation includes measurements of both pitch ($\mathbf{\Theta}$) and yaw ($\mathbf{\Psi}$) deformation angles using strain-gauge sensors installed on the cross-spring pivot leaves and the measurement of both pitch ($\mathbf{K}_{\mathbf{\Theta}}\mathbf{\Theta}$) and yaw ($\mathbf{K}_{\mathbf{\Psi}}\mathbf{\Psi}$) pivot moments using the balance cell installed at the rear, between the sting and nacelle. Propeller and motor-related quantities include the propeller $\mathbf{\Omega}$, torque (\mathbf{M}_k) and the immediate power (\mathbf{P}) that are evaluated by the servo amplifier. The propeller thrust (\mathbf{T}) is measured by the single component balance cell. Wind-tunnel related quantities include the angle of manipulator ($\mathbf{\Theta}_m$), airflow velocity (\mathbf{V}) and dynamic pressure (\mathbf{q}). The system is controlled by the special in-house LabVIEW-based SW tool. Mechanical concept of the nacelle is shown in figure 4 that shows the uncoated nacelle with the description of parts. Figure 5 shows the state with blocked yaw and pitch degrees-of-freedom.

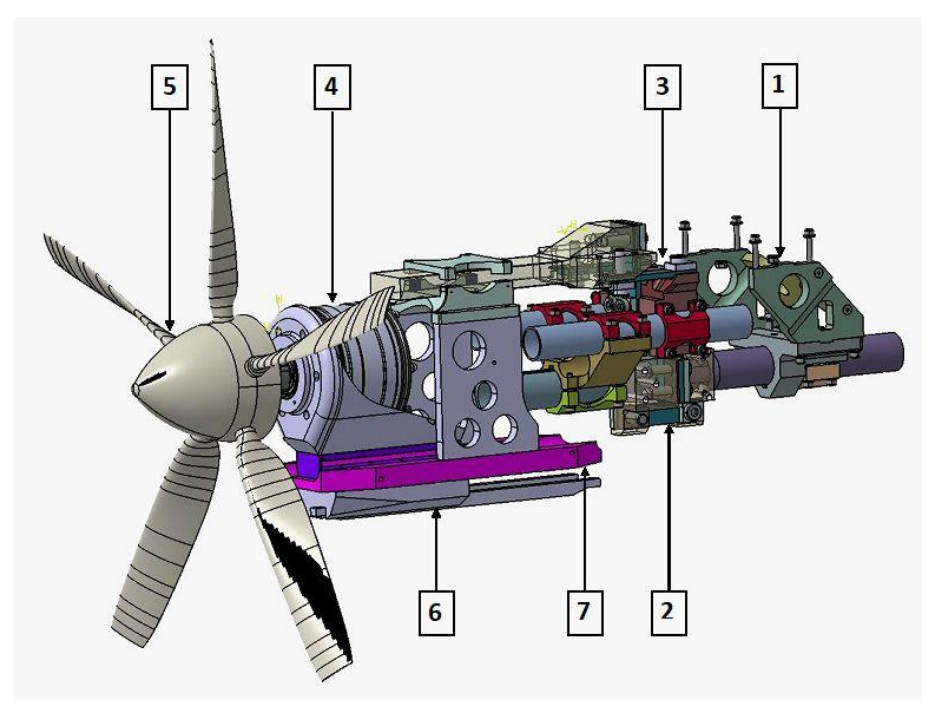


Figure 4: W-STING demonstrator, uncoated nacelle with motor and propeller (1 – sting attachment; 2 – yaw attachment; 3 – pitch attachment; 4 – motor; 5 – propeller; 6 – massbalance weight; 7 – thrust measurement cell).

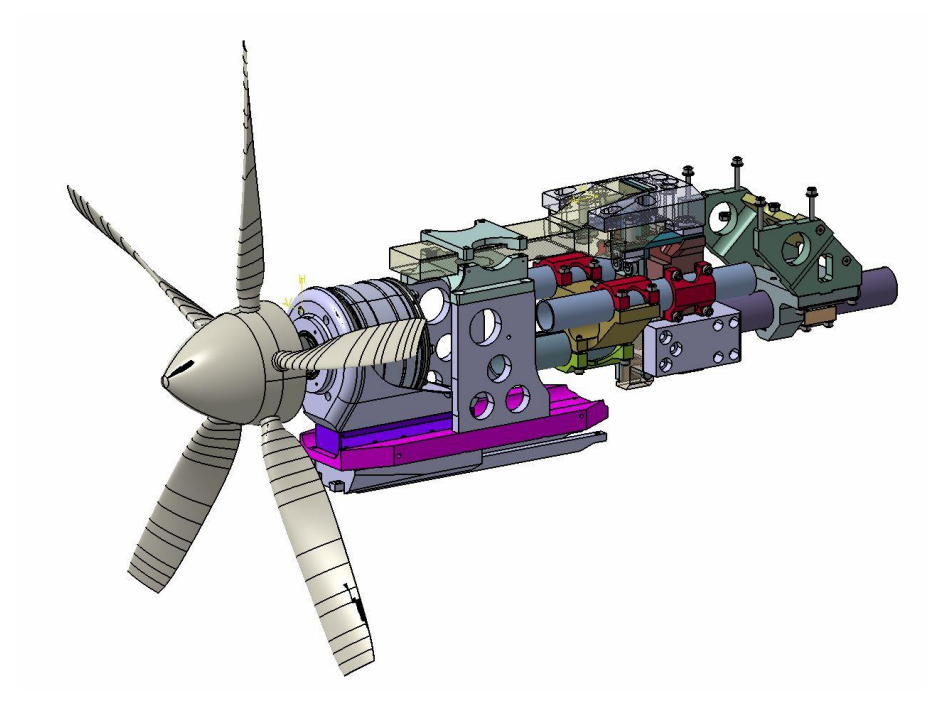


Figure 5: W-STING demonstrator, uncoated nacelle with motor and propeller, blocked yaw, and pitch degree-of.freedom.

4. Aerodynamic Derivatives Assessment Methodology

The static equations for the engine and propeller pitch and yaw deflection may be (from eqn. 1) expressed using the total moment-related derivatives (denoted by *) as:

$$k^2\Theta = \kappa(c_{m\Theta}^*\Theta + c_{m\Psi}^*\Psi) \qquad \qquad k^2\Psi = \kappa(c_{n\Psi}^*\Psi + c_{n\Theta}^*\Theta)$$
 (6)

Note that the relations $c_{m\Theta}^* = c_{n\Psi}^*$ and $c_{m\Psi}^* = -c_{n\Theta}^*$ given by eqn. 4 were used in the latter equation. For determination of $c_{m\Theta}$ (pitch moment due to pitch angle) and $c_{z\Theta}$ (vertical force due to pitch angle) derivatives, the pitch-only arrangement of the demonstrator is used. Hence, for $\Psi = 0$, the total pitching moment coefficient (c_m^*) may be expressed as:

$$c_m^* = (K_\Theta \Theta / qSD) \tag{7}$$

Where $\mathbf{K}_{\Theta}\Theta$ is the measured pitch pivot moment. The measurement is performed varying the pitch angle (by manipulator) and the moment is evaluated with respect to the pitch angle (Θ). The slope of the measured curves is the reference total pitch moment due to pitch angle derivative ($\mathbf{c}_{m\Theta}^*$). To separate the force and moment contributions to the total pitch moment, two configurations varying the distance between the gimbal axis and the propeller plane (\mathbf{a}) are measured. The equations are:

$$c_{m\Theta 1}^* = c_{m\Theta} - (a_1/D)c_{z\Theta}$$
 $c_{m\Theta 2}^* = c_{m\Theta} - (a_2/D)c_{z\Theta}$ (8)

And the final expressions for the aerodynamic derivatives become:

$$c_{m\Theta} = (1/(a_2 - a_1))(a_2 c_{m\Theta 1}^* - a_1 c_{m\Theta 2}^*) \qquad c_{z\Theta} = (D/(a_2 - a_1))(c_{m\Theta 1}^* - c_{m\Theta 2}^*)$$
(9)

For determination of $\mathbf{c}_{m\Psi}$ (pitch moment due to yaw angle) and $\mathbf{c}_{z\Psi}$ (vertical force due to yaw angle) derivatives, the yaw-only arrangement of the demonstrator is used. Hence, the total yawing moment coefficient (\mathbf{c}_{n}^{**}) may be expressed as:

$$c_n^{**} = (K_{\Psi} \Psi / qSD) = (c_{n\Psi}^* \Psi + c_{n\Theta}^* \Theta)$$
 (10)

Where $\mathbf{K}_{\Psi}\Psi$ is the measured yaw pivot moment. The measurement is performed varying the pitch angle (by manipulator) and the moment is evaluated with respect to this pitch angle (Θ) . The slope of the measured curves $(c_{n\Theta}^{**})$ and eqn. (9) are used to obtain the reference yaw total moment due to pitch angle derivative $(c_{n\Theta}^{*})$ that is:

$$c_{n\Theta}^* = (c_{n\Theta}^{**} - c_{n\Psi}^*(\Psi/\Theta))$$
 (11)

The yaw-to-pitch angle ratio (Ψ/Θ) is constant just for a given blade angle and dynamic pressure. Since the (Ψ/Θ) ratio is dynamic pressure dependent, the yawing moment coefficient (c_n^{**}) is dynamic pressure dependent as well. The reference total yaw moment due to yaw angle derivative $(c_{n\Psi}^{*})$ is obtained using the antisymmetry (eqn. (4)) as $c_{n\Psi}^{*} = c_{m\Theta}^{*}$. Similarly, we use $c_{n\Theta}^{*} = -c_{m\Psi}^{*}$ to obtain the reference total pitch moment due to yaw angle derivative $(c_{m\Psi}^{*})$. Separation of $(c_{m\Psi}^{*})$ to its components $(c_{m\Psi})$ and $(c_{z\Psi})$, i.e., the separation of force and moment contributions is carried out similarly as mentioned above, i.e., by measuring of two configurations varying the distance between the gimbal axis and the propeller plane (a). The final expressions for aerodynamic derivatives are:

$$c_{m\Psi} = (1/(a_2 - a_1))(a_1 c_{n\Theta 2}^* - a_2 c_{n\Theta 1}^*) \qquad c_{z\Psi} = (D/(a_2 - a_1))(c_{n\Theta 2}^* - c_{n\Theta 1}^*)$$
 (12)

5. Test Arrangement and Measured Configurations

For the measurement, the blocking of either pitch or yaw movement is provided. Pitching moment due to the pitch angle $(c_{m\Theta})$ and vertical force due to the pitch angle $(c_{r\Theta})$ derivatives are measured using pitch-only model arrangement. Pitching moment due to the yaw angle $(c_{m\Psi})$ and vertical force due to the yaw angle $(c_{r\Psi})$ derivatives are measured using yaw-only model arrangement. Moment at the active gimbal axis (pitch or yaw) is measured for the variable pitch angles that are provided by the movement of the manipulator within the range of -20 deg and +20 deg. From the slope of the measured curves, the reference (pitch or yaw) moment coefficient is evaluated. For the yaw movement active, the dynamic pressure dependent yaw-to-pitch angle ratio must be also considered. To separate the contributions of both force and moment to the total moment and to evaluate the final derivatives, the measurement of two configurations varying the distance between the gimbal axis and the propeller plane is used.

With respect to the above-described methodology of assessment of aerodynamic derivatives, the test plan included four basic groups of measurements:

- 1) Pitch degree-of-freedom active, front pivot station.
- 2) Yaw degree-of-freedom active, front pivot station.
- 3) Pitch degree-of-freedom active, rear pivot station.
- 4) Yaw degree-of-freedom active, rear pivot station.

Where the pitch and yaw hinge stations are:

Pitch pivot station: rear ($\mathbf{a} = 533.0 \text{ mm}$; $\mathbf{a/R} = 1.523$), front ($\mathbf{a} = 417 \text{ mm}$; $\mathbf{a/R} = 1.191$).

Yaw pivot station: rear ($\mathbf{a} = 581.5 \text{ mm}$; $\mathbf{a}/\mathbf{R} = 1.661$), front ($\mathbf{a} = 477.5 \text{ mm}$; $\mathbf{a}/\mathbf{R} = 1.364$).

In the above-mentioned four groups, changes of secondary parameters are realized. The tested variants include:

Pitch stiffness, yaw stiffness: 1 choice, thickness of cross-springs $\mathbf{t} = 3.0 \text{ mm}$.

Weight station: 1 choice, rear.

Choice of propeller: 1 choice, duralumin blades.

Blade angle of attack ($\beta_{0.75R}$): 2 choices, 5 deg, 10 deg.

Propeller revolutions (Ω): 3 choices, windmilling, 3600 rpm and 4200 rpm.

Airflow velocity (V): 10 m/s, 20 m/s and 30 m/s.

The choices of parameters described form 54 variants in total. In 8 ones, the propeller did not show the positive thrust, therefore, these ones were excluded. Finally, 46 measurement runs were realized. The wind tunnel test arrangement is documented in figures 6 to 9.



Figure 6: W-STING demonstrator, wind tunnel test arrangement, manipulator angle 0 deg.

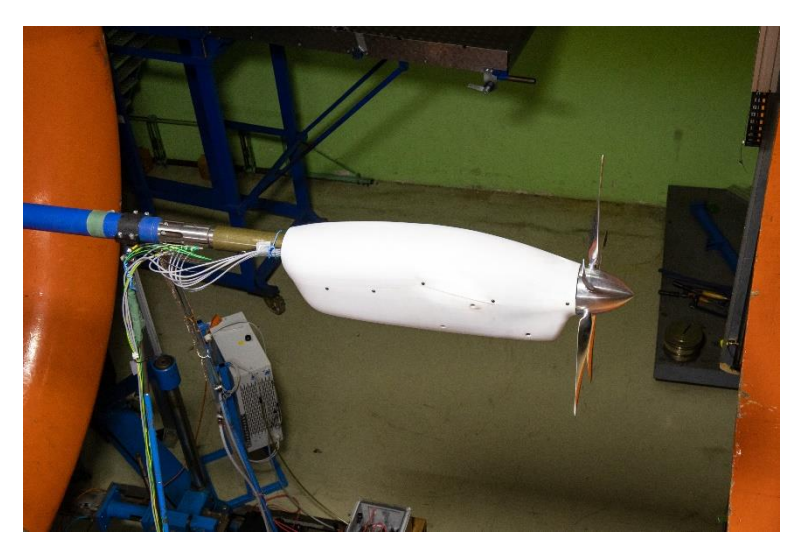


Figure 7: W-STING demonstrator, wind tunnel test arrangement, nacelle detail.



Figure 8: W-STING demonstrator, wind tunnel test arrangement, manipular angle 20 deg.

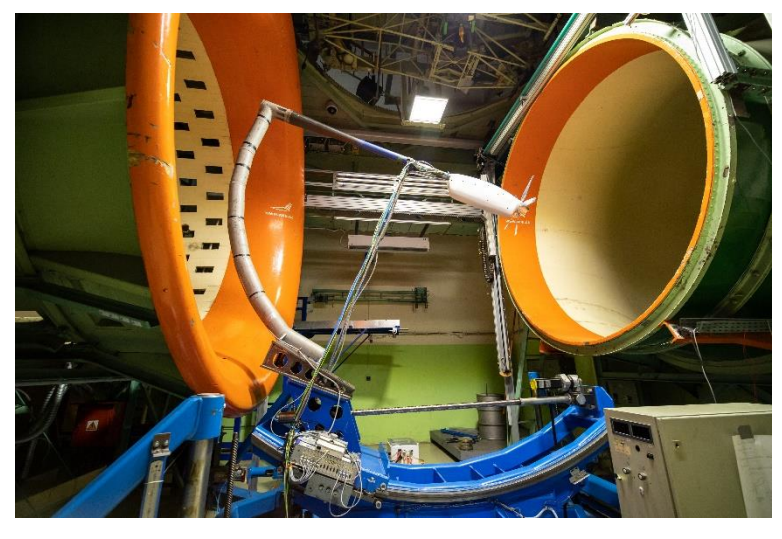


Figure 9: W-STING demonstrator, wind tunnel test arrangement, manipular angle -20 deg.

6. Test Results

The final results include the following aerodynamic derivatives:

Pitch force due to pitch angle $(c_{z\Theta})$,

Pitch moment due to pitch angle $(c_{m\Theta})$,

Pitch force due to yaw angle $(c_{z\Psi})$,

Pitch moment due to yaw angle $(c_{m\Psi})$.

The other four derivatives can be obtained from (anti)symmetry:

Yaw force due to yaw angle $(-c_y\Psi)$,

Yaw moment due to yaw angle $(c_n \Psi)$,

Yaw force due to pitch angle $(c_{y\Theta})$,

Yaw moment due to pitch angle $(-c_{n\Theta})$.

As an example, $c_{m\Theta}$ and $c_{m\Psi}$ derivatives are presented in figures 10 and 11. The curves represent the measured variants in terms of the propeller revolutions (windmilling, 3600 rpm and 4200 rpm) and the blades' angle of attack (5 and 10 deg.).

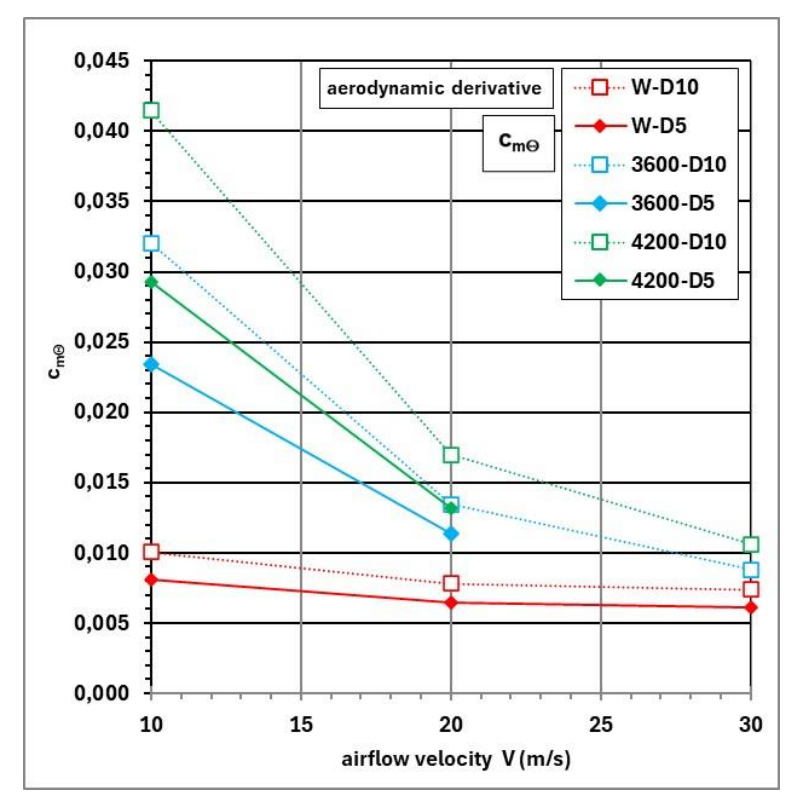


Figure 10: Aerodynamic derivative $c_{m\Theta}$.

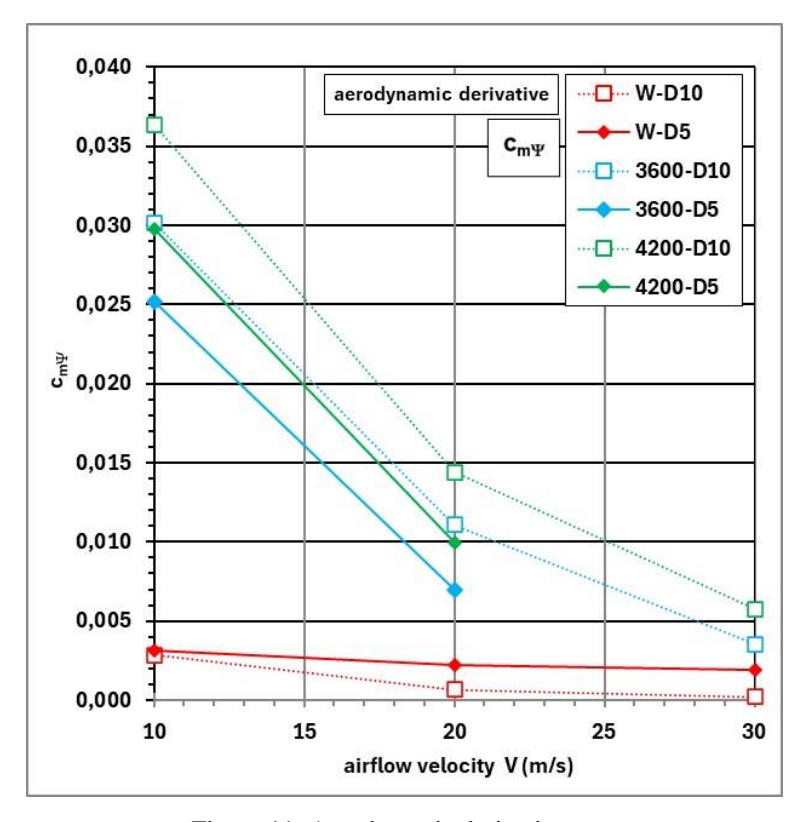


Figure 11: Aerodynamic derivative $c_{m\Psi}$.

The figures 12 to 15 demonstrate the evaluation of derivatives using the slopes of the pitch or yaw moment coefficients. The presented curves represent the blade angle of attack of 5 and 10 deg. and the states of front and rear hinge station and the pitch and yaw degree-of-freedom active (FP, RP, FY, RY).

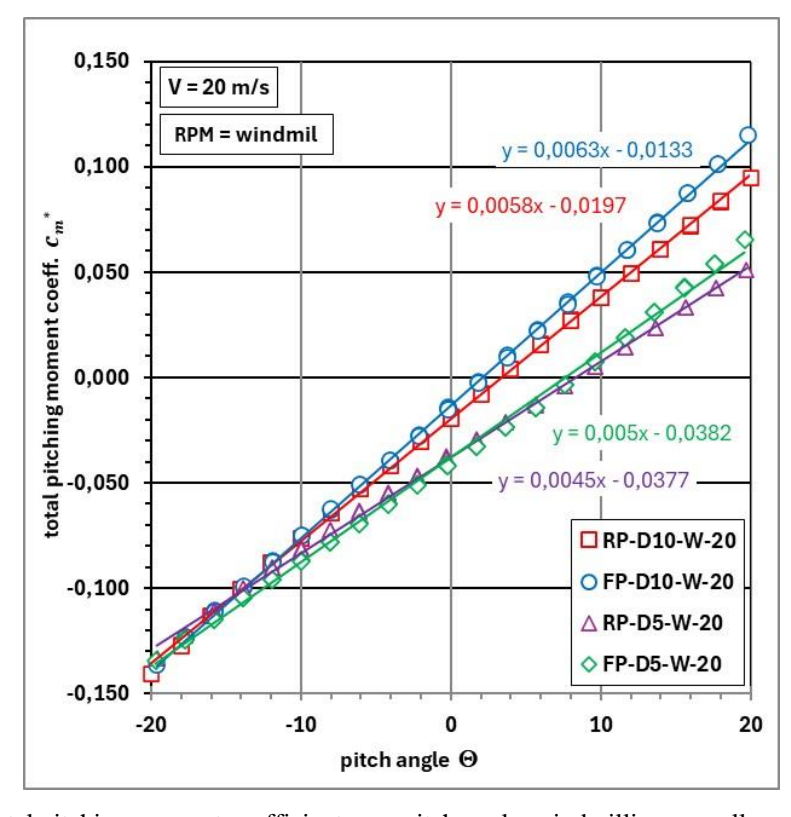


Figure 12: Total pitching moment coefficient over pitch angle, windmilling propeller, airflow 20 m/s.

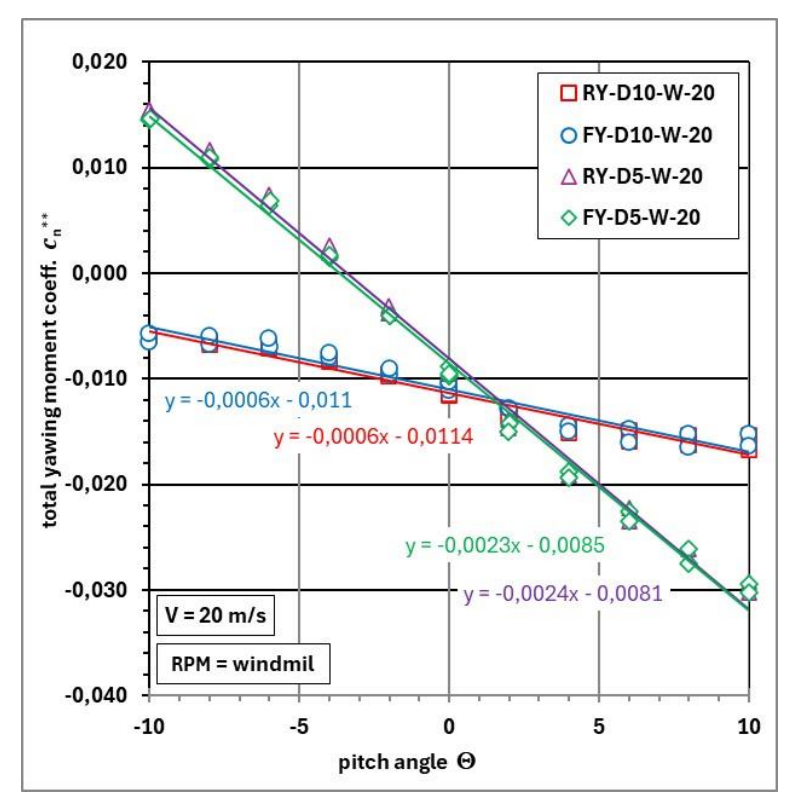


Figure 13: Total yawing moment coefficient over pitch angle, windmilling propeller, airflow 20 m/s.

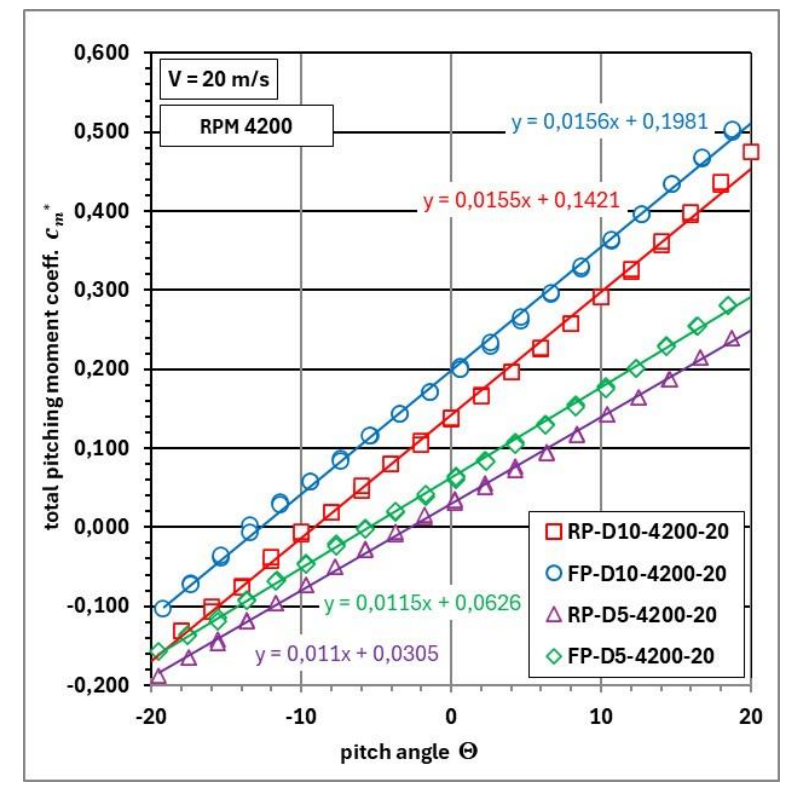


Figure 14: Total pitching moment coefficient over pitch angle, propeller revolutions 4200 rpm, airflow 20 m/s.

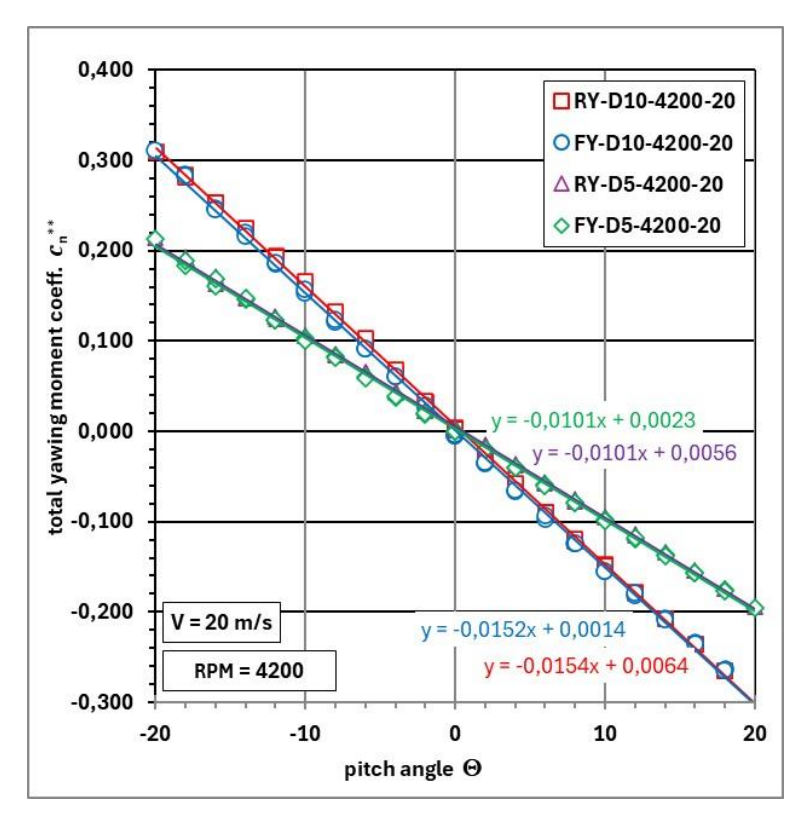


Figure 15: Total yawing moment coefficient over pitch angle, propeller revolutions 4200 rpm, airflow 20 m/s.

As an example of the secondary results, the propeller thrust over the pitch angle for the case of $\Omega = 4200$ rpm and V = 20 m/s is presented in figure 16. The presented curves represent the blade angle of attack of 5 and 10 deg. and the states of front and rear hinge station.

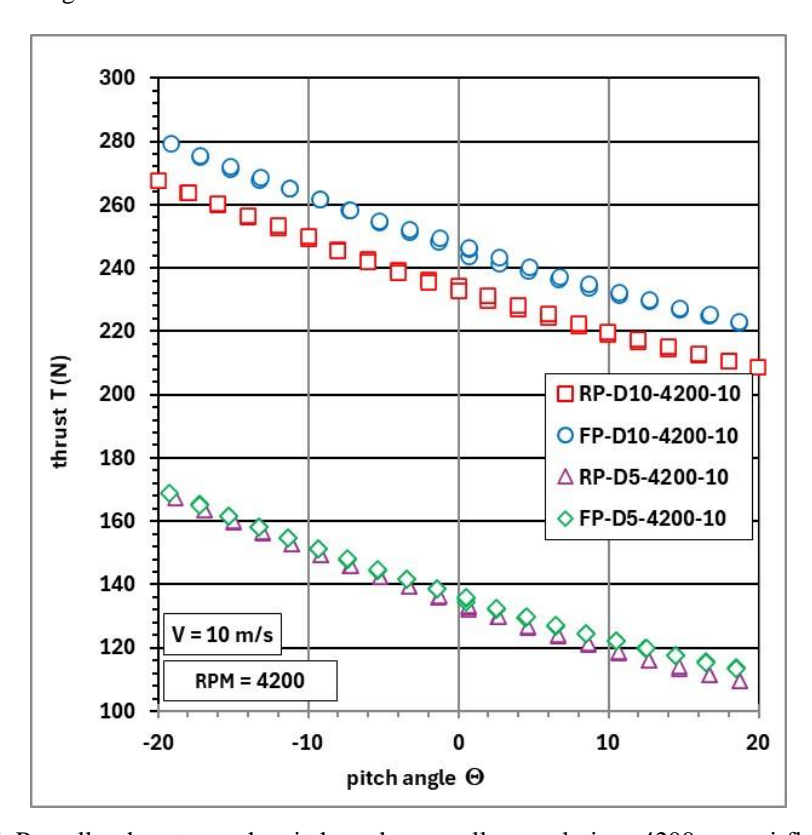


Figure 16: Propeller thrust over the pitch angle, propeller revolutions 4200 rpm, airflow 20 m/s.

7. Conclusion

The paper deals with the experimental assessment of the propeller aerodynamic derivatives. The used demonstrator represents a sting-mounted nacelle with the engine and thrusted propeller. The demonstrator's concept allows adjusting of all main parameters influencing whirl flutter. A broad testing campaign in the VZLU 3m-diameter wind tunnel was accomplished. The test schedule included the measurement of four aerodynamic derivatives. Secondary variable parameters included the airflow velocity (dynamic pressure), propeller revolutions and the blades' angle of attack. The experimental results will be subsequently utilised for verification of the analytical models and computational tools [17, 18] that will be used for development of the new power plant system, characterised as an open-fan concept, utilised for a new generation short-medium range turboprop aircraft.

Acknowledgement

Program and topic: HORIZON-JU-CLEAN-AVIATION-2022-01-SMR-01, Ultra Efficient Propulsion Systems for Short and Short-Medium Range Aircraft. Project nr. and title: 101102011, Open Fan for Environmental Low Impact of Aviation (OFELIA).

References

- [1] Taylor, E. S., and Browne, K. A. 1938. Vibration Isolation of Aircraft Power Plants, J. Aerosp. Sci., 6(2):43-49.
- [2] Ribner, H. S. 1945. Propellers in Yaw, NASA Rep. 820.
- [3] Ribner, H. S. 1945. Formulas for Propellers in Yaw and Charts of the Side Force Derivatives, NACA Rep. 819.
- [4] Donham, R. E. and Watts, G. A. 1997. Whirl Flutter First Case, In: The Revolution in Structural Dynamics, (Editor Dr. Hugh Flomenhoft), Dynaflo Press, Palm Beach Gardens, FL, USA, 99-109.
- [5] Reed, W. H., and Bland, S. R. 1961. An Analytical Treatment of Aircraft Propeller Precession Instability, NASA TN D-659.
- [6] Reed, W. H. and Bennett, R. M. 1963. Propeller Whirl Flutter Considerations for V/STOL Aircraft, In: *CAL/TRECOM Symposium*, Buffalo, NY, USA.
- [7] Bland, S. R. and Bennett, R. M. 1963. Wind-Tunnel Measurement of Propeller Whirl-Flutter Speeds and Static Stability Derivatives and Comparison with Theory, NASA TN D-1807.
- [8] Bennett, R. M. and Bland, S. R. 1964. Experimental and Analytical Investigation of Propeller Whirl Flutter of a Power Plant on a Flexible Wing, NASA TN D-2399.
- [9] Abbott, F.T., Jr., Kelly, H. N., Hampton, K. D. 1963. Investigation of Propeller-Power Plant Autoprecession Boundaries for a Dynamic-Aeroelastic Model of a Four-Engine Turboprop Transport Airplane, NASA, Technical Note, TN D-1806.
- [10] Kvaternik, R. G., and Kohn, J. S. 1977. An Experimental and Analytical Investigation of Proprotor Whirl Flutter, NASA TP 1047.
- [11] Krishna Rao, K. V. and Sundararajan, D. 1969. Whirl Flutter of Flapping Blade Rotor Systems, NAL TN-18, National Aeronautical Laboratory, Bangalore, India.
- [12] Čečrdle, J. 2023. Whirl Flutter of Turboprop Aircraft Structures, 2nd Ed., Elsevier Science, Oxford, UK.
- [13] Čečrdle, J. and Maleček, J. 2013. Mechanical Concept of W-WING Whirl Flutter Aeroelastic Demonstrator, *Proc. Institution of Mech. Engineers, Part G: J. Aerosp. Eng.*, 229(8):1485-1494.
- [14] Čečrdle, J. Malínek, P. and Vích, O. 2017. Wind Tunnel Test of a Whirl Flutter Aeroelastic Demonstrator, In: *Proc. AIAA SciTech Forum*, San Diego, CA, USA.
- [15] Čečrdle, J. Vích, O. and Malínek, P. 2019. Wind Tunnel Test of a Whirl Flutter Aeroelastic Demonstrator, *Proc. Institution of Mech. Engineers, Part G: J. Aerosp. Eng.*, 233(3):969-977.
- [16] Houbolt, J. C. and Reed, W. H. 1962. Propeller Nacelle Whirl Flutter, J. Aerosp. Sci., 29:333-346.
- [17] Dugeai, A., Mauffrey, Y. and Sicot, F. 2011. Aeroelastic Capabilities of the elsA Solver for Rotating Machines Applications, In: *Int. Forum on Aeroelasticity and Structural Dynamics*, Paris, France.
- [18] Sicot, F. and Dugeai, A. 2011. Numerical Investigation of Propellers Whirl Flutter Using elsA, In: *Int. Forum on Aeroelasticity and Structural Dynamics*, Paris, France.